Accepted Manuscript

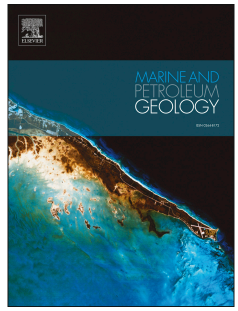

The shallow depth emplacement of mafic intrusions on a magma-poor rifted margin: An example from the Bight Basin, Southern Australia

P. Reynolds, S. Holford, N. Schofield, A. Ross

PII: S0264-8172(17)30358-6

DOI: 10.1016/j.marpetgeo.2017.09.008

Reference: JMPG 3066

To appear in: *Marine and Petroleum Geology*

Received Date: 9 June 2017

Revised Date: 5 September 2017

Accepted Date: 8 September 2017

Please cite this article as: Reynolds, P., Holford, S., Schofield, N., Ross, A., The shallow depth emplacement of mafic intrusions on a magma-poor rifted margin: An example from the Bight Basin, Southern Australia, *Marine and Petroleum Geology* (2017), doi: 10.1016/j.marpetgeo.2017.09.008.

The shallow depth emplacement of mafic intrusions on a magma-poor rifted margin: an example from the Bight Basin, southern Australia

P. Reynolds[1*], S. Holford[1], N. Schofield[2], A. Ross[3]

[1] Centre for Tectonics, Resources and Exploration (TRaX), Australian School of Petroleum, University of Adelaide, Adelaide, SA 5005, Australia

[2]Department of Geology & Petroleum Geology, University of Aberdeen, Aberdeen AB24 3UE, UK

[3]CSIRO Energy, Australian Resources Research Centre, 26 Dick Perry Avenue, Kensington, WA 6151, Australia

*Corresponding author: peter.reynolds@adelaide.edu.au, +61484607355

Abstract

Three-dimensional (3D) seismic data has provided important insights into how magma is transported and stored in sedimentary basins. Much of our understanding is based on volcanic-rifted margins. In contrast, the magma plumbing systems of magma-poor rifted margins are less well studied. This study uses 3D seismic data to describe the magma plumbing system of the Bight Basin Igneous Complex; a volcanic province located along the magma-poor southern Australian margin. Here, magma emplacement occurred in the Mid Eocene, some 40 million years after the onset of seafloor spreading. Our data images a variety of 30−270 m thick, 2−23 km diameter mafic intrusions that are confined to within 1200 m of the paleoseabed. Intrusions emplaced at ≤200 m depth formed hybrid and compound sills and are typified by elongate, lava flow-like morphologies. Intrusions emplaced at depths of 200−1200 m formed saucer-shaped and compound sills, as well as laccoliths. Approximately 60% of the intrusions have lava flows and volcanogenic vents above their shallowest tips, as shown from previous studies. This suggests that the intrusions played a crucial role in transporting magma to the paleoseabed. Furthermore, many of the intrusions are overlain by forced folds, highlighting the role of magma emplacement in inducing overburden deformation. Contrary to observations from volcanic rifted margins, the sills and laccoliths rarely form interlinked complexes. Instead, they most commonly occur as isolated bodies. This suggests that the sills and laccoliths were fed by dykes. We infer that high rates of magma ascent in the dykes prevented their transition into sills within sediments at >1.2 km depth. Our study highlights that the magma plumbing system of the Bight Basin Igneous Complex contains a diversity of magmatic intrusions, the morphology of which is linked to their emplacement depth, host sediment rheology and the physical properties of the magma. This plumbing system contrasts markedly with those found along better-studied volcanic rifted margins.

1. Introduction

Sills and laccoliths play an important role in transporting and storing mafic magma in the shallow crust (Thomson, 2007; Muirhead et al., 2014; Magee et al., 2016). These features can form vertically and laterally connected complexes capable of facilitating magma movement for tens of kilometres through the crust (e.g. Thomson and Hutton, 2004; Planke et al., 2005; Cartwright and Hansen, 2006; Polteau et al., 2008; Schofield et al., 2015). From a volcanological perspective, sills and laccoliths are important because they can feed eruptions and modulate eruptive activity (e.g. Magee et al., 2013; Magee et al., 2016; Muirhead et al., 2016; Reynolds et al., 2016; Magee et al., 2017). As summarised by Magee et al. (2016), sills also provide insights into continental rifting, the thermomechanical state of the mantle and the physiochemical evolution of magma. Furthermore, mafic intrusions have been hypothesised to play an important role in driving global climate change, since work from the North Atlantic has shown that the emplacement of mafic intrusions into carbon-rich sediments can cause the release of greenhouse gases (e.g. Svensen et al., 2004; Reynolds et al., 2017).

Sills and laccoliths also have a range of implications for petroleum systems (e.g. Senger et al., 2017). For instance, these intrusions can act as barriers and/or conduits to fluid flow in the subsurface (e.g. Rateau et al., 2013; Schofield et al. 2015; Schofield et al. 2017) as well as hydrocarbon reservoirs (Rodriguez Monreal et al., 2009). Furthermore, magma intrusion is often associated with source rock maturation (Rodriguez Monreal et al., 2009) and the formation of forced folds (e.g. Pollard and Johnson, 1973; Jackson and Pollard, 1990; Trude et al., 2003; Schmiedel et al, 2017). These folds can be used to elucidate the timing of magmatism, as well as potentially acting as traps for hydrocarbons (Trude et al., 2003; Schutter 2003; Holford et al., 2012).

Many observations of magma plumbing systems are from volcanic rifted margins which contain abundant mafic intrusions (e.g. Thomson and Hutton, 2004; Planke et al., 2005; Cartwright and Hansen, 2006; Schofield et al., 2015; Reynolds et al., 2017). However, since many of the intrusions along these margins are deeply buried, they often cannot be imaged at high resolution; partly as a result of decreasing seismic frequency with depth. Furthermore, many intrusions along volcanic rifted margins are located beneath thick sequences of extrusive volcanic rocks (e.g. Seaward Dipping Reflectors and Landward Flows) further obscuring intrusion distribution and morphology (e.g. Symonds et al., 1998; Planke et al., 2000; Reynolds et al., 2017). In contrast, there are comparatively few studies of the magma plumbing systems along magma-poor rifted margins (e.g. Autin et al., 2010; Franke et al., 2014; Peace et al., 2017). Therefore, our understanding of the emplacement mechanisms and controls on magma plumbing system formation along these margins is not well understood.

In this study, we use 3D seismic data from the magma-poor southern Australian margin. This data allows us to detail how magma was transported and stored in a sedimentary basin that has undergone volcanic activity not intrinsically linked to continental rifting. Our unique dataset images intrusions buried beneath a shallow (<2 km) sequence of sedimentary rocks. The shallow emplacement depth of the intrusions and absence of Seaward Dipping Reflections and Landward Flows (typical of volcanic rifted margins) also means our data is of high resolution, allowing the complexities of intrusion emplacement to be investigated in detail. Although focused on the southern Australian margin, our findings have implications for understanding the emplacement of magmatic intrusions in sedimentary basins along other continental rifted margins.

2. Geological setting

The Ceduna sub-basin is located within the Bight Basin on the southern margin of Australia (Fig. 1). The sub-basin has an area of 90,000 km^2 and contains over 15 km of syn and post-rift Mesozoic sedimentary rocks (Totterdell and Krassay, 2003; MacDonald et al., 2010). These rocks are sub-divided into a series of supersequences that were deposited from the mid- to late-Jurassic onwards. The earliest of these sequences record slow thermal subsidence, whilst the Late Santonian-aged Tiger Supersequence records increases in subsidence rate deposited the during major marine flooding (Totterdell et al., 2000). This supersequence is composed of marginal marine to marine mudstones (Totterdell et al., 2000). Deposition of these mudstones correlates with upper crustal extension and formation of large, east-west striking faults and re-activation of Cenomanian growth faults (Robson et al., 2016).

The overlying Ceduna Delta succession was deposited from the Late Santonian onwards, and is composed of the Hammerhead Supersequence (Totterdell et al., 2000; MacDonald et al., 2013). Component sedimentary rocks are characteristic of marine, deltaic and coastal plain environments, and were deposited during extremely low spreading rates of <100 m year (Tikku and Cande, 1999). The Gnarlyknots-1A petroleum exploration well penetrated this supersequence and encountered water-saturated sandstones and shales, interpreted to form as shallow marine prograding delta top sets (Totterdell et al., 2000; Tapley et al., 2005).

Both the Hammerhead and the overlying Wobbegong sequences (deposited following a 5−7 Myr hiatus) are dissected by northwest-southeast oriented Cenomanian-Santonian and Campanian-Maastrichtian-aged normal faults, formed during gravity-driven extension of the delta (Robson et al., 2016). The overlying Dugong Supersequence is dominated by cool water carbonates that developed on a carbonate shelf and contains minor amounts of sandstones at its base (Totterdell et al., 2000; Macdonald et al., 2012). This supersequence formed from the middle Eocene onwards during a period of fast seafloor spreading and records a marine transgression with water depths of up 300 m (Li et al., 2003).

The southern margin of Australia is also characterised by an abundance of both offshore and onshore igneous rocks (e.g. Holford et al., 2012; Jackson, 2012; Cas et al., 2016; Meeuws et al., 2016; Reynolds et al., 2016). Melt production along the southern Australian margin has been proposed to result from processes similar to those in intraplate volcanic provinces, such as mantle shearing, mantle plumes and small scale convection above steps in lithospheric thickness (Demidjuk et al., 2007; Conrad et al., 2011; Davies et al., 2015). Subsequent volcanism may be associated with the onset of rapid spreading in the mid Eocene and reconfigurations of the Indo-Australian plate boundaries (Holford et al., 2012).

The subject of this study is a 9000 km^2 area within the ~130 km diameter Bight Basin Igneous Complex (BBIC). This complex is found in the centre of the Ceduna sub-basin (Fig. 1). Previous work based on the Flinders 2D seismic survey has shown that the BBIC contains intrusions, lava flows, volcanogenic vents and forced folds (Schofield and Totterdell, 2008; Jackson et al., 2013; Magee et al., 2013). These features are described below.

Jackson et al. (2013) suggested that the intrusions range from 7−19 km in diameter and 32−250 m in thickness. Their morphologies have previously been divided into sill, laccolith and hybrid types (Jackson et al., 2013). Intrusions are found within the Wobbegong, Hammerhead and Tiger Supersequences (Figs. 1 and 2; see also Schofield and Totterdell, 2008). Many of the intrusions are overlain by forced folds which reach 17 km in width and display up to 210 m of relief (Jackson et al., 2013). These folds are interpreted to have formed as a result of magma emplacement in the subsurface since they directly overly the intrusions. The folds typically have reliefs lower than the thickness of the underlying intrusion, suggesting fluidisation and expulsion of pore fluids from the host rock accompanied elastic bending of the overburden (Jackson et al., 2013). The Dugong Supersequence onlaps the folds, indicating the intrusions were emplaced in the Mid-Eocene (Schofield and Totterdell, 2008; Jackson et al., 2013; Magee et al., 2013).

A total of 56 vents were identified by Magee et al. (2013). The vents downlap the top of the mid Eocene-aged Wobbegong Supersequence and are onlapped by the Dugong Supersequence (Schofield and Totterdell, 2008; Jackson et al., 2013; Magee et al., 2013). They typically overly the shallowest tips of underlying intrusions. The vents range from 1.09−18.89 km in diameter, and have been interpreted as hydrothermal vents and shield volcanoes (Magee et al., 2013). The vents and volcanoes have been distinguished based on morphological characteristics such as their flank dip, summit height and seismic velocity. The spatial and temporal relationship between the vents and intrusions suggest that they are genetically linked (Magee et al., 2013). Dredging from incised canyons collected detrital volcanic fragments that were characterised as amygdaloidal, possibly pillowed, alkali basalts (Clarke and Alley, 1993) suggesting that the vents have a similar composition (Schofield and Totterdell, 2008; Magee et al., 2013). The vents occur on the same horizon as biogenic mounds, which are distinguished based on their lower lateral variation in seismic amplitude, higher internal continuity, smaller heights and the absence of wash-out beneath (Langhi et al., 2016).

3. Method and dataset

This study uses the Nerites 3D and Flinders 2D seismic reflection surveys (Fig. 1). The Nerites survey covers an area of 9000 km^2 and extends to 9 s depth, of which the top 3 s were used in this study. This dataset has a bin spacing of 12.5 m × 15 m. The Flinders survey covers 44,000 km^2 and also extends to 9 s depth. The 2D lines are spaced 4−8 km. Data are displayed with an SEG reverse polarity; a downward increase in acoustic impedance (i.e. hard event) is measured by a trough and is represented by a blue reflection. The seismic surveys are tied to the Gnarlyknots-1A and Potoroo-1 wells using the Flinders 2D seismic survey. The wells are located 65 km and 175 km to the northwest of the Nerites survey. Neither well penetrated the intrusions, therefore we assumed a velocity of 5500 m s^{-1} (Planke et al., 2005) to calculate their thicknesses. Although typical for many intrusions (e.g. Skogly, 1998; Hansen and Cartwright, 2006), this value represents a lower estimate for the velocity of the intrusions; Nelson et al. (2009) record values up to 7000 m s^{-1}. The resolution and detection limit of the seismic data were calculated using a frequency of 30 Hz, which is the dominant frequency of the Nerites survey at the level at which the intrusions were mapped (between 2.1−2.8 s). Assuming a velocity of 5500 m s^{-1}, this indicates the intrusions must be ≥5 m to be detected and ≥45 m thick to be resolved. Based on the potential variation in their velocity (e.g. Nelson et al., 2009), these values likely represent the minimum thicknesses that can be detected and resolved.

3.1 Seismic interpretation strategy

In order to determine the vertical and lateral distribution of the intrusions, and their relationship to the lava flows, volcanogenic vents and paleoseabed, we mapped each of these features throughout the Nerites survey. Our interpretation strategy is outlined below.

3.1.1 Mapping of the paleoseabed

The Base Dugong (BD) reflection represents the paleoseabed at the time of volcanism (Schofield and Totterdell, 2008; Jackson et al., 2013; Magee et al., 2013). It is represented by a moderate-high amplitude, trough event that forms a prominent unconformity that is onlapped by the overlying Dugong Supersequence. The BD is downlapped by the vents and is folded above underlying intrusions.

3.1.2 Mapping of volcanogenic vents and lava flows

The tops of the volcanogenic vents are represented by the Top Vent (TV) reflection. This reflection varies from low to high amplitude and from a trough to peak event. It varies in character from smooth to rough and continuous to semi-continuous. The vents are onlapped by the overlying Dugong Supersequence which may be domed above the centre of the vent. In time slice the vents have a concentric structure which becomes more chaotic with depth. The bases of the vents are represented by the BD reflection and/or the top of an adjacent vent in cases where vents overlap. Seismic velocity "pull-up" and washout is common beneath the vents, particularly towards their centres (e.g. Schofield and Totterdell, 2008; Magee et al., 2013). Such features are typical of volcanic rocks in sedimentary sequences (e.g. Jerram, 2002)

The tops of the lava flow fields are represented by the Top Extrusive (TE) reflection. This is represented by a high amplitude trough that is parallel to the underlying BD reflection. The

TE reflection is smooth, sub horizontal and terminates abruptly. Seismic velocity pull-up and zones of washout are common beneath the TE.

3.1.3 Mapping of intrusions

We mapped the intrusions using the seismostratigraphic approach of Planke et al. (2000) and Planke et al. (2015). The top of the intrusions are represented by the Top Intrusion (TI) reflection. Intrusions can split into several units or merge, meaning that the TI reflection is located at multiple levels and is not laterally continuous. It is a high amplitude, trough event that cross-cuts adjacent reflections and has abrupt terminations. The Base Intrusion (BI) reflection is a moderate-high amplitude, peak event that also cross-cuts adjacent reflections and has abrupt terminations. In regions where the Base Intrusion reflection was not visible (i.e. the thickness of the intrusion is below the resolution limit of the data) the intrusion was represented by a single trough-peak doublet. In this case, we picked the peak event of the doublet as the Base Intrusion.

3.2 Calculating intrusion emplacement depth and volume

The emplacement depth of the intrusions was calculated from the distance in milliseconds two-way time (TWT) between the TI reflection and the BD reflection. We converted from TWT to depth in metres using an interval velocity of 2100 m s^{-1}, as indicated by the Gnarlyknots-1A well.

For each intrusion we calculated a minimum and maximum volume from depth-converted grids of the Top Intrusion and Base Intrusion reflections. In the first instance, these calculations assume that the intrusions have a thickness equal to the seismic detection limit (5 m) in regions where the intrusion was represented by a single trough-peak doublet. Conversely, to calculate the maximum volumes, we assumed that the intrusions have a thickness of 44 m (the maximum possible thickness below the resolution limit) in regions where the only a single trough-peak doublet was identified. Since the entire thicknesses of some intrusions are between the detection limit and resolution limit, they have a wide range in possible volumes (e.g. intrusion 1, Table 1). In contrast, other intrusions are >45 m in thickness across 90% of their areas, giving them a narrow volume range (e.g. intrusion 4, Table 1).

4. Description of the intrusions

4.1 Intrusion morphology

Four morphologically-distinct types of intrusions are identified, including saucer-shaped, compound and hybrid sills, as well as laccoliths (Fig. 3). All intrusions occur 100−1200 m beneath the paleoseabed (not accounting for compaction) within the Tiger, Hammerhead and Wobbegong Supersequences (Fig. 4). These intrusions vary from 2−23 km in length, 1−18 km in width and 5−270 m in thickness (Figs. 4 and 5). Their morphology is described below.

4.1.1 Saucer-shaped sills

Saucer-shaped sills comprise half of all mapped intrusions. They have a sub-circular shape in plan view whilst in cross section they have a flat inner saucer and gently inclined, transgressive rims defined by sub-parallel TI and BI reflections (Fig. 3). The inner saucers form 60−70% of the sills' diameter, whilst the rims make up the remaining 30−40%. These rims can transgress the host rocks by up to 225 m (e.g. intrusion 26; Fig. 3). The sills have volumes varying from 0.01−3.03 km^3 (Table 1). Their thicknesses vary from 5−160 m and their thickest regions are found in the centre of the inner saucer (Fig. 5).

4.1.2 Compound intrusions

Compound intrusions constitute approximately 10% of the mapped intrusions. They are commonly elongate and have convex or concave, irregular-shaped margins in plan view (Fig. 3). Compound intrusions have volumes of <0.01−13.39 km^3 (Table 1) and vary from 5−150 m thick. The intrusions may have multiple regions >45 m thick (Fig. 5) and these regions commonly occur at the greatest depths (300 m). Seismic amplitude maps indicate that the compound intrusions are composed of multiple lobes which vary from elongate to saucer-shaped. This is typified by intrusion 31, which is composed of multiple lobes approximately 1−8 km in diameter (measured along their longest axis). These lobes have convex or concave margins and aspect ratios of 1−4. In cross section, the lobes have convex-up, convex-down or planar-shaped geometries defined by the TI reflection (Fig. 3). This reflection is paralleled by the BI reflection (Fig. 3).

4.1.3 Hybrid Intrusions

Hybrid intrusions account for approximately a third of the magmatic bodies in the Nerites survey. In plan view, the hybrid intrusions are typically elongate, and those emplaced at <200 m depth have sinuous, "lava flow-like" morphologies (e.g. intrusion 36; Fig. 3). Their volumes vary from 0.04−10.41 km^3 (Table 1). The hybrid intrusions vary from 5−190 m thick, and thin towards their distal margins (Fig. 5). The thickest regions occurring above their deepest parts. As for the compound intrusions, seismic amplitude maps indicate that these intrusions are composed of multiple lobes. Some lobes are sub-circular with transgressive rims (e.g. intrusion 20; Fig. 4) whilst others are more elongate (e.g. intrusion 36; Fig. 3). The longest axes of individual lobes vary from 0.4−14 km in diameter, and they have aspect ratios of 1−8. The lobes shallow towards their distal margins. In cross section the lobes have convex-up or down shapes TI reflections which are paralleled by their BI reflections (Fig. 3).

4.1.4 Laccoliths

The laccoliths represent 5% of the intrusions in the Nerites survey. In plan view the laccoliths are elongate. They have volumes varying from 7.24−10.93 km^3 and thicknesses varying from 5−270 m. The thickest parts of the laccoliths are found along their central axes (Fig. 5). Seismic amplitude maps indicate they are composed of a central, elongate lobe that bifurcates into a series of peripheral lobes that transgress the stratigraphy (Fig. 3). The lobes have convex-outwards margins. Measurements of the longest lobe axes indicate they vary from 1−13 km in length and they have aspect ratios of 1−4. The central lobes are the largest lobes. In cross section, individual lobes have a convex-upwards TI reflection and a sub-horizontal BI reflection. The lobes have sinuous amplitude anomalies along their length that run parallel to the lobes' longest axis (Fig. 3). These anomalies terminate abruptly at lobe junctions.

4.2 Intrusion distribution and connectivity

The intrusions are concentrated in the inboard, central part of the Ceduna sub-basin above the Potoroo fault system (Fig. 1). The intrusions were emplaced at depths ranging from 100−1200 m, with the shallowest intrusions tending to be found basinward (Figs. 4 and 6). There appears to be no relationship between intrusion diameter and emplacement depth; large diameter intrusions can occur at all depths in the survey (Fig. 6). Saucer-shaped sills are found at the greatest depths of all the intrusion types, and occur 60−1200 m beneath the paleoseabed. Saucer-shaped sills >1 km^3 in size are only found at depths >500 m (e.g. intrusions 6 and 12). The hybrid intrusions and compound intrusions are found at the shallowest depths of 60−1000 m and 180−880 m respectively. These intrusions display no relationship between volume and emplacement depth (Fig. 6). Laccoliths are found at

260−1200 m depth and they similarly do not display a volume-depth relationship. Many of the intrusions are overlain by forced folds (Schofield and Totterdell, 2008; Jackson et al., 2013; Magee et al., 2013). The outlines of these folds are similar to that of the underlying intrusion, and their amplitudes are equal-to or lower than the thickness of the underlying intrusion (Jackson et al., 2013).

About 60% of the intrusions are not vertically or laterally connected to others, and occur as isolated features (e.g. intrusions H7 and H18; Fig. 7; Table 1). The remaining 40% of the intrusions form interlinked complexes. These complexes are composed of individual intrusions which overlap by as much as half of their diameter (e.g. Intrusions 12 and 24; Fig. 7). The complexes can extend laterally for 20 km and vertically for ~600 m. The intrusions do not offset each other, preventing deduction of the relative timing of intrusion emplacement.

4.3 Determining intrusion source regions

The morphology of the intrusions and their component lobes are similar to those of other mafic intrusions identified from 3D seismic and well data (e.g. Planke et al., 2005; Schofield et al., 2012a; Schofield et al., 2015). We are able to use the morphology of the intrusions (e.g. bridge structures; see Schofield et al., 2012a) and their emplacement depths to infer the direction of magma flow. Mafic intrusions usually propagate from their deepest parts towards the paleosurface (see Galland et al., 2009; Schofield et al., 2010). Magma is also commonly transported from larger "feeder" lobes towards smaller lobes at the periphery of the intrusion (e.g. Schofield et al., 2012a; Suleiman et al., 2017). Based on these observations, we infer that the saucer-shaped sills were emplaced via flow of magma upwards and radially outwards from a source region found at their deepest points (e.g. Fig. 8; Malthe-Sørenssen et al., 2004; Galland et al., 2009). In comparison, the compound sills are characterised by radial and unidirectional magma flow in their component lobes (Fig. 8). We suggest that these intrusions were constructed via the amalgamation of multiple lobes fed from multiple points, rather than by the "feeding" of one lobe to another, as within the saucer-shaped sills. Magma flow in the hybrid intrusions was strongly unidirectional in the elongate lobes, whilst was radial in their sub-circular lobes. Similar to the saucer-shaped sills, these intrusions have a source region located at their deepest point (Fig. 8). Within the laccoliths, the direction of magma flow appears to have been predominantly unidirectional from a source point at their greatest depth (Fig. 8).

4.4 The role of dykes in feeding the sills and laccoliths

We interpret that many of the intrusions are fed by dykes (e.g. Fig. 9) since the sills and laccoliths most commonly occur as isolated features that do not form vertically connected complexes. Approximately half of the dykes are inferred to have propagated up both north-dipping and south-dipping fault planes, supported by the location of approximately half of the intrusions' source regions above fault planes (e.g. Fig. 8). The dykes intruded and were emplaced approximately perpendicular to the regional orientation of σ_3, as indicated by their orientation within east-west striking normal faults. We infer that the remaining half of the dykes propagated via host-rock fracturing at the dyke tip and did not exploit pre-existing faults. The possibility of the dykes exploiting faults within the wash out zones beneath the intrusions is excluded, since many faults have lengths of 50 km; greater than the diameters of overlying intrusions (≤23 km). The length of the dykes is unknown; dykes do not propagate to equal heights along their length (Keating et al., 2008). Our observations therefore complement those of other intraplate volcanic provinces, which suggest that dykes form the dominant mechanism of vertical magma transport (e.g. Brenna et al., 2011; van den Hove et al., 2017).

5. Relationship between intrusive and extrusive components of the magmatic system

5.1 The surface manifestation of volcanism

The BBIC contains lava flow fields and volcanogenic vents that are most densely concentrated within the central part of the Nerites survey (Figs. 1 and 10). These features onlap onto the forced folds (Fig. 11). In our dataset, approximately 60% of the vents and lava flow fields are found directly above the tips of the sills and laccoliths (Fig. 12). The remaining extrusive features are either not underlain by intrusions (20% of those mapped; Fig. 10) or are found above the centres of compound intrusions (20% of those mapped; Fig. 10).

5.2 The role of intrusions in feeding surface volcanism

A temporal link between the timing of intrusive and extrusive activity is evidenced by the extrusive features which onlap onto the forced folds caused by the intrusions, and the fact that the forced folds, vents and lava flows are all onlapped by the Dugong Supersequence (Figs. 11 and 12). The spatial relationship between the extrusive features and the shallowest, lateral terminations of intrusions (e.g. Fig. 12) leads us to suggest that the sills and laccoliths played an important role in feeding eruption sites and delivering magma to the paleoseabed, consistent with previous authors (Magee et al., 2013). Whilst we cannot prove that each individual extrusive feature was directly fed by the intrusion which it overlies, the intrusions which terminate within 100 m of the BD provide strong evidence that some vents and lava flow fields were fed by the underlying intrusion. Small dykes emanating from sill tips may have facilitated magma movement in the shallowest subsurface. Consistent with Magee et al. (2013) we infer that the tips of intrusions may not be imaged in contact with the base of the overlying vents because either: 1) the volcanoes were fed by dykes in the shallowest hundreds of metres, and these dykes cannot be imaged in seismic data (e.g. Thomson, 2007); and/or 2) washout of seismic data beneath the volcanoes prevents us from imaging the shallowest tips of the intrusions.

It is interesting that some of the intrusions are not linked to any extrusive features (e.g. intrusion 37; Fig. 10). This suggests that not all intrusions acted as magma conduits to the paleoseabed and simply represent stalled bodies of magma. Conversely, the absence of concordant intrusions beneath some extrusive features suggests that dykes, not imaged in our data set, also delivered magma directly to the paleoseabed. This further highlights the importance of dykes as a method of magma transport within the BBIC.

6. Magma emplacement in the Bight Basin Igneous Complex

6.1 Controls on intrusion emplacement depth

Intrusions imaged within the Nerites survey are emplaced at shallow depths (<1200 m; not accounting for compaction). These intrusions have by-passed a number of rheological interfaces and shale-rich horizons (e.g. within the Pre-Campanian sequences; see Totterdell et al., 2000) which are commonly favoured by sills (Schofield et al. 2012b). This observation suggests that contrasting rigidity and/or the host rock rheology did not control the depth of intrusion emplacement, as reported by other authors (e.g. Kavanagh et al., 2006; Gudmundsson, 2011; Menand, 2011). However, previous work has shown that the dyke-sill transition can be suppressed at mechanical interfaces if magma ascends at sufficiently high rates (Chanceaux and Menand, 2014). Therefore, we infer that the vertical distribution of the intrusions in the Nerites survey results from the dykes which fed the sills and laccoliths ascending at rapid rates and by-passing the deeper (>1.2 km depth) sediments. As magma approached the paleosurface its' ascent rate slowed (e.g. Taisne and Jaupart, 2011) there-by increasing the probability of sill formation at shallow depths.

Evidence of high magma ascent rates is found onshore along the southern Australian margin, where magma transited from the mantle to the surface in 1−10 days. This implies magma ascent rates of >10 cm s^{-1} (Holt et al., 2013; Van Otterloo et al., 2014). High magma ascent rates are also recorded in other NVP volcanoes (Van Otterloo et al., 2014) and other intraplate volcanic fields (e.g. McGee et al., 2011). Our study therefore supports the conclusions of Holt et al. (2013) who suggested that volcanic provinces characterised by high magma ascent rates have plumbing systems found within the shallowest sections of the crust.

An additional influence on the depth of dyke-sill transition may be the orientation of principal stresses. At depths >1200 m, the vertical principal stress is σ_2, thus favouring dyke intrusion. In contrast, at shallow depths, the principal stress changes to σ_3, favouring sill intrusion. The effects of stress orientation could have acted in tandem with the effects of magma ascent speed and have facilitated restriction of the dyke-sill transition to depths <1200 m. However, we are unable to account for why some dykes were able to ascend directly to the surface feeding the vents, whilst others fed sills and laccoliths.

Other authors infer the dyke-sill transition can be initiated by asperities and lithological contrasts across fault planes (Valentine and Krogh, 2006), causing local rotation of principal stresses (Chester and Chester, 2000). However, in the Ceduna sub-basin, the fault planes cross numerous lithological boundaries at depth, and therefore does not provide a satisfactory explanation for why the sill-dyke transition occurred at such shallow depths. The level of neutral buoyancy is not thought to have been important in controlling the dyke-sill transition, because the sills are found at multiple stratigraphic horizons, and fed eruptions at the paleoseabed. Numerous other studies of intrusions within sedimentary basins (e.g. Thomson, 2007) and numerical models (e.g. Maccaferri et al., 2011) also suggest that the level of neutral buoyancy plays a relatively minor role in determining the dyke-sill transition.

6.2 Lava-like intrusions: characteristic features of shallow depth magma emplacement?

In our study, the hybrid intrusions with sinuous, lava flow-like shapes are restricted to shallow (<200 m) depths (e.g. intrusions 36, 37, 39). Other authors have similarly reported that intrusions emplaced in the shallowest hundreds of metres of sedimentary basins have lava flow-like morphologies (e.g. Fig. 13; Trude, 2004; Hansen and Cartwright, 2006; Miles and Cartwright, 2010). The lava flow-like shapes of the hybrid intrusions contrasts markedly with the saucer-shaped sills and laccoliths, which are typical morphologies for intrusions emplaced at depths of a few hundred metres or more (e.g. Planke et al., 2005; Polteau et al., 2008; Schofield et al., 2012b). These combined observations therefore suggest that lava flow-like sills represent a unique intrusion morphology that is characteristic of shallow depth magma intrusion (Fig. 14).

We infer that the lava flow-like intrusions were dominantly emplaced by ductile mechanisms. This hypothesis is supported by data from the Gnarlyknots-1A well (see section 2) which indicates that the sediments within the Hammerhead Supersequence were water-saturated and had anomalously high porosity; conditions which favour ductile magma emplacement (Schofield et al., 2012b). Previous authors have focused on the importance of host rock rheology in controlling intrusion morphology (e.g. Schofield et al. 2010; Miles and Cartwright, 2010; Schofield et al. 2012b). In contrast, factors such as magma emplacement rate, emplacement duration and the physical properties of the magma have previously been neglected. However, these factors play an important role in governing the emplacement of lava flow fields (e.g. Hon et al., 1994; Soule et al., 2004). Although we cannot quantify these processes, we suggest that they are likely to play an increasingly dominant role in magma emplacement at shallow depths (Fig. 14).

6.3 Comparison with volcanic rifted margins

In our study, many of the intrusions are of small volume (<14 km^3), were emplaced at shallow depths (<1200 m) and are not laterally and vertically interconnected. This is in contrast to those found along volcanic rifted margins which are 10's of km diameter and are found at depths ranging from <1−9 km (Planke et al., 2005; Schofield et al., 2015; Reynolds et al., 2017). These sills often form interconnected complexes (e.g. Planke et al., 2005; Schofield et al., 2015; Magee et al., 2016; Reynolds et al., 2017) and are capable of transporting magma vertically and laterally for 12 km and 4100 km respectively (Cartwright and Hansen, 2006; Magee et al., 2016).

There are several factors which could account for the differing magma plumbing systems in the BBIC and those along volcanic rifted margins. As described in Section 6.1, we infer that the vertical distribution of the sills and laccoliths in this study partially results from dykes that ascended through the lithosphere at high rates. Magma ascent rate may therefore have also played a role in controlling the emplacement depth of sills along volcanic rifted margins. Although not well studied, magma ascent rate may have also influenced whether interlinked complexes of sills developed, as suggested by Magee et al., (2016) and references there-in. The volume of magma intruded may also partially influenced whether inter-linked sill complexes form; intrusions with as larger diameter are more likely to become inter-connected than smaller diameter intrusions (see also Holt et al., 2013).

In summary, whilst factors such as host rock lithology and elastic mismatch no doubt play an important role in governing the vertical distribution and interconnectedness of magmatic intrusions in sedimentary basins (see Magee et al., 2016 for a thorough review), our study highlights the potentially important role of magma ascent rate and magma volume in influencing the architecture of magma plumbing systems in sedimentary basins.

7. Conclusions

We have shown that the Bight Basin Igneous Complex, offshore southern Australia, contains a variety of saucer-shaped, compound and hybrid sills, as well as laccoliths. Our 3D seismic data indicates that these intrusions were emplaced within 1200 m of the paleoseabed and are overlain by a series of forced folds, volcanogenic vents and lava flow fields. The spatial linkage between the lava flow fields and vent suggests that the intrusions played an important role in delivering magma to the paleoseabed. Many of the intrusions occur as isolated bodies, suggesting that they were fed by dykes. We infer that high magma ascent rates enabled magma propagating in dykes to bypass lithological interfaces, resulting in focusing of the intrusions in the shallow subsurface. Our study indicates that magma-poor rifted margins are characterised by a diversity of shallow-depth, dyke-fed intrusions, the manifestation of which is controlled intrinsic magma properties (e.g. ascent and emplacement rate, volume and physical properties) as well as host rock lithology.

8. References

Autin, J., Leroy, S., Beslier, M. O., d'Acremont, E., Razin, P., Ribodetti, A., & Al Toubi, K., 2010, Continental break-up history of a deep magma-poor margin based on seismic reflection data (northeastern Gulf of Aden margin, offshore Oman): Geophysical Journal International, v. 180, no. 2, p. 501-519.

Brenna, M., Cronin, S. J., Németh, K., Smith, I. E. M., and Sohn, Y. K., 2011, The influence of magma plumbing complexity on monogenetic eruptions, Jeju Island, Korea: Terra Nova, v. 23, no. 2, p. 70-75.

Cartwright, J., and Møller Hansen, D., 2006, Magma transport through the crust via interconnected sill complexes: Geology, v. 34, no. 11, p. 929-932.

Cas, R., van Otterloo, J., Blaikie, T., and van den Hove, J., 2016, The dynamics of a very large intra-plate continental basaltic volcanic province, the Newer Volcanics

Province, SE Australia, and implications for other provinces: Geological Society, London, Special Publications, v. 446, p. SP446. 448.

Chanceaux, L., and Menand, T., 2014, Solidification effects on sill formation: An experimental approach: Earth and Planetary Science Letters, v. 403, p. 79-88.

Chester, F. M., and Chester, J. S., 2000, Stress and deformation along wavy frictional faults: Journal of Geophysical Research: Solid Earth, v. 105, no. B10, p. 23421-23430.

Clarke, J., and Alley, N., Petrologic data on the evolution of the Great Australian Bight, *in* Proceedings Proceedings of the Gondwana Eight Symposium: Rotterdam, AA Balkema1993, p. 585-596.

Conrad, C. P., Bianco, T. A., Smith, E. I., and Wessel, P., 2011, Patterns of intraplate volcanism controlled by asthenospheric shear: Nature Geoscience, v. 4, no. 5, p. 317-321.

Davies, D., Rawlinson, N., Iaffaldano, G., and Campbell, I., 2015, Lithospheric controls on magma composition along Earth/'s longest continental hotspot track: Nature, v. 525, no. 7570, p. 511-514.

Demidjuk, Z., Turner, S., Sandiford, M., George, R., Foden, J., and Etheridge, M., 2007, U-series isotope and geodynamic constraints on mantle melting processes beneath the Newer Volcanic Province in South Australia: Earth and Planetary Science Letters, v. 261, no. 3, p. 517-533.

Franke, D., Savva, D., Pubellier, M., Steuer, S., Mouly, B., Auxietre, J. L., & Chamot-Rooke, N., 2014, The final rifting evolution in the South China Sea: Marine and Petroleum Geology, v. 58, p. 704-720.

Galland, O., Planke, S., Neumann, E.-R., and Malthe-Sørenssen, A., 2009, Experimental modelling of shallow magma emplacement: application to saucer-shaped intrusions: Earth and Planetary Science Letters, v. 277, no. 3, p. 373-383.

Gudmundsson, A., 2011, Deflection of dykes into sills at discontinuities and magma-chamber formation: Tectonophysics, v. 500, no. 1, p. 50-64.

Hansen, D. M., and Cartwright, J., 2006, Saucer-shaped sill with lobate morphology revealed by 3D seismic data: implications for resolving a shallow-level sill emplacement mechanism: Journal of the Geological Society, v. 163, no. 3, p. 509-523.

Holford, S., Schofield, N., MacDonald, J., Duddy, I., and Green, P., 2012, Seismic analysis of igneous systems in sedimentary basins and their impacts on hydrocarbon prospectivity: examples from the southern Australian margin, The APPEA Journal, v. 52, no. 1, p. 229-252.

Holt, S., Holford, S., and Foden, J., 2013, New insights into the magmatic plumbing system of the South Australian Quaternary Basalt province from 3D seismic and geochemical data: Australian Journal of Earth Sciences, v. 60, no. 8, p. 797-817.

Hon, K., Kauahikaua, J., Delinger, R., and Mackay, K., 1994, Emplacement and inflation of pahoehoe sheet flows: Observations and measurements of active lava flows on Kilauea Volcano, Hawaii: Geological Society of America Bulletin, v. 106, no. 3, p. 351-370.

Jackson, M. D., and Pollard, D. D., 1990, Flexure and faulting of sedimentary host rocks during growth of igneous domes, Henry Mountains, Utah. Journal of Structural Geology 12.2: 185-206.

Jackson, C. A., 2012, Seismic reflection imaging and controls on the preservation of ancient sill-fed magmatic vents. Journal of the Geological Society v. 169, no. 5, p. 503-506.

Jackson, C. A., Schofield, N., and Golenkov, B., 2013, Geometry and controls on the development of igneous sill–related forced folds: A 2-D seismic reflection case study from offshore southern Australia: Geological Society of America Bulletin, v. 125, no. 11-12, p. 1874-1890.

Jerram, D. A., 2002, Volcanology and facies architecture of flood basalts: Geological Society of America Special Papers, v. 362, p. 119-132.

Kavanagh, J. L., Menand, T., and Sparks, R. S. J., 2006, An experimental investigation of sill formation and propagation in layered elastic media: Earth and Planetary Science Letters, v. 245, no. 3, p. 799-813.

Keating, G., Valentine, G., Krier, D., and Perry, F., 2008, Shallow plumbing systems for small-volume basaltic volcanoes: Bulletin of Volcanology, v. 70, no. 5, p. 563-582.

Langhi, L., Strand, J., and Ross, A. S., 2016, Fault-related biogenic mounds in the Ceduna Sub-basin, Australia. Implications for hydrocarbon migration: Marine and Petroleum Geology, v. 74, p. 47-58.

Li, Q., James, N., and McGowran, B., 2003, Middle and Late Eocene Great Australian Bight lithobiostratigraphy and stepwise evolution of the southern Australian continental margin: Australian Journal of Earth Sciences, v. 50, no. 1, p. 113-128.

Maccaferri, F., Bonafede, M., and Rivalta, E., 2011, A quantitative study of the mechanisms governing dike propagation, dike arrest and sill formation: Journal of Volcanology and Geothermal Research, v. 208, no. 1, p. 39-50.

Macdonald, J., Backé, G., King, R., Holford, S., and Hillis, R., 2012, Geomechanical modelling of fault reactivation in the Ceduna Sub-basin, Bight Basin, Australia: Geological Society, London, Special Publications, v. 367, no. 1, p. 71-89.

MacDonald, J., King, R., Hillis, R., and Backé, G., 2010, Structural style of the White Pointer and Hammerhead delta-deepwater fold-thrust belts, Bight Basin, Australia, The APPEA Journal, v. 50, no.1, p. 487-510.

MacDonald, J. D., Holford, S. P., Green, P. F., Duddy, I. R., King, R. C., and Backé, G., 2013, Detrital zircon data reveal the origin of Australia's largest delta system: Journal of the Geological Society, v. 170, no. 1, p. 3-6.

Magee, C., Bastow, I. D., de Vries, B. v. W., Jackson, C. A.-L., Hetherington, R., Hagos, M., and Hoggett, M., 2017, Structure and dynamics of surface uplift induced by incremental sill emplacement: Geology, p. G38839. 38831.

Magee, C., Hunt-Stewart, E., and Jackson, C. A.-L., 2013, Volcano growth mechanisms and the role of sub-volcanic intrusions: insights from 2D seismic reflection data: Earth and Planetary Science Letters, v. 373, p. 41-53.

Magee, C., Muirhead, J. D., Karvelas, A., Holford, S. P., Jackson, C. A., Bastow, I. D., Schofield, N., Stevenson, C. T., McLean, C., and McCarthy, W., 2016, Lateral magma flow in mafic sill complexes: Geosphere, v. 12, no. 3, p. 809-841.

Malthe-Sørenssen, A., Planke, S., Svensen, H., and Jamtveit, B., 2004, Formation of saucer-shaped sills: Physical Geology of High-Level Magmatic Systems. Geological Society, London, Special Publications, v. 234, p. 215-227.

McGee, L. E., Beier, C., Smith, I. E., and Turner, S. P., 2011, Dynamics of melting beneath a small-scale basaltic system: a U-Th–Ra study from Rangitoto volcano, Auckland volcanic field, New Zealand: Contributions to Mineralogy and Petrology, v. 162, no. 3, p. 547-563.

Meeuws, F., Holford, S., Foden, J., and Schofield, N., 2016, Distribution, chronology and causes of Cretaceous–Cenozoic magmatism along the magma-poor rifted southern Australian margin: Links between mantle melting and basin formation: Marine and Petroleum Geology, v. 73, p. 271-298.

Menand, T., 2011, Physical controls and depth of emplacement of igneous bodies: A review: Tectonophysics, v. 500, no. 1, p. 11-19.

Miles, A., and Cartwright, J., 2010, Hybrid flow sills: a new mode of igneous sheet intrusion: Geology, v. 38, no. 4, p. 343-346.

Muirhead, J. D., Airoldi, G., White, J. D., and Rowland, J. V., 2014, Cracking the lid: Sill-fed dikes are the likely feeders of flood basalt eruptions: Earth and Planetary Science Letters, v. 406, p. 187-197.

Muirhead, J. D., Eaton, A. R., Re, G., White, J. D. L., and Ort, M. H., 2016, Monogenetic volcanoes fed by interconnected dikes and sills in the Hopi Buttes volcanic field, Navajo Nation, USA: Bulletin of Volcanology, v. 78, no. 2, p. 1-16.

Nelson, C. E., Jerram, D.A and Hobbs, R. W, 2009, Flood basalt facies from borehole data: implications for prospectivity and volcanology in volcanic rifted margins. Petroleum Geoscience v.15 no.4, p. 313-324.

Peace, A., McCaffrey, K., Imber, J., Hobbs, R., van Hunen, J., and Gerdes, K., 2017, Quantifying the influence of sill intrusion on the thermal evolution of organic-rich sedimentary rocks in nonvolcanic passive margins: an example from ODP 210-1276, offshore Newfoundland, Canada: Basin Research, v. 29, no. 3, p. 249-265.

Planke, S., Rasmussen, T., Rey, S., and Myklebust, R., Seismic characteristics and distribution of volcanic intrusions and hydrothermal vent complexes in the Vøring and Møre basins, *in* Proceedings Geological Society, London, Petroleum Geology Conference series2005, v. 6, Geological Society of London, p. 833-844.

Planke, S., Svensen, H., Myklebust, R., Bannister, S., Manton, B., and Lorenz, L., 2015, Geophysics and Remote Sensing, p.1-16, doi:10.1007/11157_2014_6

Planke, S., Symonds, P. A., Alvestad, E., and Skogseid, J., 2000, Seismic volcanostratigraphy of large-volume basaltic extrusive complexes on rifted margins: J. Geophys. Res., v. 105, no. B8, p. 19335-19351.

Pollard, D D., and Johnson, A. M., 1973, Mechanics of growth of some laccolithic intrusions in the Henry Mountains, Utah, II: bending and failure of overburden layers and sill formation. Tectonophysics 18.3-4 (1973): 311-354.

Polteau, S., Mazzini, A., Galland, O., Planke, S., and Malthe-Sørenssen, A., 2008, Saucer-shaped intrusions: Occurrences, emplacement and implications: Earth and Planetary Science Letters, v. 266, no. 1–2, p. 195-204.

Rateau, R., Schofield, N., and Smith, M., 2013, The potential role of igneous intrusions on hydrocarbon migration, West of Shetland: Petroleum Geoscience, v. 19, no. 3, p. 259-272.

Reynolds, P., Planke, S., Millett, J., Jerram, D., Trulsvik, M., Schofield, N., and Myklebust, R., 2017, Hydrothermal vent complexes offshore Northeast Greenland: A potential role in driving the PETM: Earth and Planetary Science Letters, v. 467, p. 72-78.

Reynolds, P., Schofield, N., Brown, R. J., and Holford, S., 2016, The architecture of submarine monogenetic volcanoes – insights from 3D seismic data: Basin Research, doi:10.1111/bre.12230

Robson, A., King, R., and Holford, S., 2016, Structural evolution of a gravitationally detached normal fault array: analysis of 3D seismic data from the Ceduna Sub-Basin, Great Australian Bight: Basin Research doi:10.1111/bre.12191.

Rodriguez Monreal F., Villar H. J., Baudino R., Delpino D. and Zencich S., 2009, Modeling an atypical petroleum system: a case study of hydrocarbon generation, migration and accumulation related to igneous intrusions in the Neuqen Basin, Argentina: Marine and Petroleum Geology, v. 26, no. 4, p. 590-605.

Schofield, A., and Totterdell, J., 2008, Distribution, timing and origin of magmatism in the Bight and Eucla Basins, Geoscience Australia.

Schofield, N., Heaton, L., Holford, S. P., Archer, S. G., Jackson, C. A.-L., and Jolley, D. W., 2012a, Seismic imaging of 'broken bridges': linking seismic to outcrop-scale investigations of intrusive magma lobes: Journal of the Geological Society, v. 169, no. 4, p. 421-426.

Schofield, N., Holford, S., Millett, J., Brown, D., Jolley, D., R. Passey, S., Muirhead, D., Grove, C., Magee, C., Murray, J., Hole, M., A.-L. Jackson, C., and Stevenson, C., 2015, Regional magma plumbing and emplacement mechanisms of the Faroe-Shetland Sill Complex: implications for magma transport and petroleum systems within sedimentary basins: Basin Research, v. 29, p. 41-63, doi:10.1111/bre.12164.

Schofield, N., Stevenson, C., and Reston, T., 2010, Magma fingers and host rock fluidization in the emplacement of sills: Geology, v. 38, no. 1, p. 63-66.

Schofield, N. J., Brown, D. J., Magee, C., and Stevenson, C. T., 2012b, Sill morphology and comparison of brittle and non-brittle emplacement mechanisms: Journal of the Geological Society, v. 169, no. 2, p. 127-141.

Schutter, S R., 2003, Hydrocarbon occurrence and exploration in and around igneous rocks. Geological Society, London, Special Publications 214.1: 7-33.

Senger, K., Millett, J., Planke, S., Ogata, K., Eide, C., Festøy, M., Galland, O., and Jerram, D., 2017, Effects of igneous intrusions on the petroleum system: a review. First Break. 35. 47-56. 10.3997/1365-2397.2017011.

Skogly, O.P., 1998, Seismic characterization and emplacement of intrusives in the Vøring Basin [Ph.D. thesis]: University of Oslo.

Soule, S. A., Cashman, K. V., and Kauahikaua, J. P., 2004, Examining flow emplacement through the surface morphology of three rapidly emplaced, solidified lava flows, Kilauea Volcano, Hawai'i: Bulletin of Volcanology, v. 66, no. 1, p. 1-14.

Suleiman, A., Magee, C., Jackson, C.-L., and Fraser, A., 2017, Igneous activity in the Bornu Basin, onshore NE Nigeria; implications for opening of the South Atlantic: Journal of the Geological Society, p. jgs2016-2107.

Svensen, H., Planke, S., Malthe-Sorenssen, A., Jamtveit, B., Myklebust, R., Rasmussen Eidem, T., and Rey, S. S., 2004, Release of methane from a volcanic basin as a mechanism for initial Eocene global warming: Nature, v. 429, no. 6991, p. 542-545.

Symonds, P. A., PLanke, S., Frey, Ø and Skogside, J., 1998, Volcanic evolution of the Western Australian continental margin and its implications for basin development. *In*: Purcell, P.G and Purcell, R.R (eds) The Sedimentary Basins of Western Australia 2: Proceedings of Petroleum Exploration Society of Australia Symposium, Perth, 33-54.

Taisne, B., and Jaupart, C., 2011, Magma expansion and fragmentation in a propagating dyke: Earth and Planetary Science Letters, v. 301, no. 1, p. 146-152.

Tapley, D., Mee, B., King, S., Davis, R., and Leischner, K., 2005, Petroleum potential of the Ceduna Sub-basin: impact of Gnarlyknots-1A: The APPEA Journal, v. 45, no. 1, p. 365-380.

Thomson, K., 2007, Determining magma flow in sills, dykes and laccoliths and their implications for sill emplacement mechanisms: Bulletin of Volcanology, v. 70, no. 2, p. 183-201.

Thomson, K., and Hutton, D., 2004, Geometry and growth of sill complexes: insights using 3D seismic from the North Rockall Trough: Bulletin of Volcanology, v. 66, no. 4, p. 364-375.

Tikku, A. A., and Cande, S. C., 1999, The oldest magnetic anomalies in the Australian-Antarctic Basin: Are they isochrons?: Journal of Geophysical Research: Solid Earth, v. 104, no. B1, p. 661-677.

Tobias, S., Sigurd, K., Planke,. S., Magee, C., Galland, O., Schofield, N., Jackson, C., and Jerram, D., 2017. Mechanisms of overburden deformation associated with the emplacement of the Tulipan sill, mid-Norwegian margin: Interpretation, v. 5, no. 3, SK23-SK38. doi.org/10.1190/INT-2016-0155.1

Totterdell, J., Blevin, J., Struckmeyer, H., Bradshaw, B., Colwell, J., and Kennard, J., 2000, Petroleum frontiers, systems and plays-A new sequence framework for the Great Australian Bight: Starting with a clean slate: APPEA Journal-Australian Petroleum Production and Exploration Association, v. 40, no. 1, p. 95-120.

Totterdell, J., and Krassay, A., 2003, The role of shale deformation and growth faulting in the Late Cretaceous evolution of the Bight Basin, offshore southern Australia: Geological Society, London, Special Publications, v. 216, no. 1, p. 429-442.

Trude, J., Cartwright, J., Davies, R. J., and Smallwood, J., 2003, New technique for dating igneous sills: Geology, v. 31, no. 9, p. 813-816.

Trude, K., 2004, Kinematic Indicators for Shallow Level Igneous Intrusions from 3D Seismic Data: Evidence of Flow Firection and Feeder Location: Geological Society, London, Memoirs, v. 29, no. 1, p. 209-218.

Valentine, G. A., and Krogh, K. E., 2006, Emplacement of shallow dikes and sills beneath a small basaltic volcanic center–The role of pre-existing structure (Paiute Ridge, southern Nevada, USA): Earth and Planetary Science Letters, v. 246, no. 3, p. 217-230.

van den Hove, J., Grose, L., Betts, P. G., Ailleres, L., Van Otterloo, J., and Cas, R. A. F., 2017, Spatial analysis of an intra-plate basaltic volcanic field in a compressional tectonic setting: South-eastern Australia: Journal of Volcanology and Geothermal Research, v. 335, p. 35-53.

Van Otterloo, J., Raveggi, M., Cas, R., and Maas, R., 2014, Polymagmatic activity at the monogenetic Mt Gambier Volcanic Complex in the Newer Volcanics Province, SE Australia: new insights into the occurrence of intraplate volcanic activity in Australia: Journal of Petrology, v. 55, no. 7, p. 1317-1351.

Figure Captions

Fig. 1. Map showing the location of the study area along the southern Australian margin and a stratigraphic column indicating that the intrusions are of Mid Eocene age.

Fig. 2. Composite seismic section using lines 43, 58, 85 and 92r from the Flinders 2D seismic survey. Uninterpreted version provided in Supplementary Data (Fig. S1).

Fig. 3. Seismic cross sections through intrusion number S13, a saucer-shaped sill (A); intrusion number C27, a compound sill (B); intrusion number H36, hybrid sill (C) and intrusion number L4; a laccolith (D). Emplacement depth and amplitude maps are also shown. See Figure 4 for their locations.

Fig. 4. Map showing the emplacement depth of the intrusions beneath the paleoseabed (the Base Dugong reflection).

Fig. 5. Map showing the thickness variation within the intrusions.

Fig. 6 Graphs showing the relationship between intrusion emplacement depth and distance towards break-up axis (A), diameter and emplacement depth (B) and volume and emplacement depth (C).

Fig. 7. Seismic cross sections of sills 7 and 18 (A) and 12 and 24 (B). In A, the intrusions overlap but are not connected. These intrusions are typical of those within the Ceduna Sub-basin. In the B the sills form a complex, perhaps allowing lateral and vertical transport of magma.

Fig. 8. Map showing the direction of magma flow within the intrusions and their source regions.

Fig. 9. 3D visualisation of a hybrid sill (number H20) showing time (A) and amplitude (B) maps and interpreted magma flow directions. The intrusion overlies a fault and is interpreted to have been fed by a dyke. See Fig. 8 for location.

Fig. 10. Map showing the distribution of vents, lava flow fields and intrusions.

Fig. 11. Seismic cross section showing a vent onlapping onto forced folds above an intrusion, indicating that intrusive activity pre-dated eruption. See Fig. 10 for location.

Fig. 12. Seismic section showing a saucer-shape sill and volcanogenic vents. The left-most vent is located above the shallowest termination of the sill ~200 m beneath the paleosurface. See Fig. 10 for location.

Fig. 13. Outlines of the Krafla lava flow, Iceland (A), intrusion 36 from this study (B, emplacement depth ~100 m) and an intrusion offshore Norway emplaced at 200−400 m depth (C; redrawn from Miles and Cartwright, 2010). The arrows indicate the direction of lava/magma flow. Note the similar sinuous morphologies and ragged terminations of each feature.

Fig. 14. Schematic diagram illustrating the factors influencing intrusion morphology, and how emplacement processes vary with emplacement depth. Adapted from Schofield et al. (2012b).

Acknowledgements

This work comprises a part of the Great Australian Bight Deepwater Marine Program (GABDMP) for funding this project. The GABDMP is a CSIRO research program, sponsored by Chevron Australia the results of which will be made publically available. 3D seismic data was gratefully provided by TGS. Dougal Jerram and Craig Magee are thanked for constructive reviews; Adam Bumby is thanked for editorial handling.

Intrusion number	Intrusion type	Is the intrusion part of a complex?	Length (km)	Width (km)	Aspect ratio	Emplacement depth (m)	Min volume* (km^3)	Max volume† (km^3)
1	Hybrid	No	4	2.1	0.5	244	0.04	0.31
2	Hybrid	No	10	5.5	0.6	533	0.86	2.35
3	Saucer	Yes	5	2.6	0.5	297	0.09	0.45
4	Laccolith	No	18	7.8	0.4	297	7.24	7.90
5	Saucer	No	3	1.9	0.6	418	0.02	0.18
6	Saucer	No	4	2.7	0.7	418	0.77	0.84
7	Hybrid	No	12	8.1	0.7	358	7.40	7.71
8	Saucer	No	9	6.9	0.8	1180	0.60	1.92
9	Hybrid	No	9	5.9	0.7	1005	2.71	3.29
10	Saucer	No	4	3	0.8	528	0.60	0.76
11	Laccolith	No	19.5	9.3	0.5	320	10.36	10.93
12	Saucer	Yes	4.8	2.4	0.5	533	0.06	0.53
13	Saucer	Yes	6	4.5	0.8	480	1.41	1.73
14	Hybrid	No	4	1	0.3	822	0.01	0.11
15	Hybrid	No	3	2.4	0.8	1119	0.46	0.47
16	Compound	No	23	12	0.5	884	13.04	13.39
17	Hybrid	Yes	8	3.1	0.4	61	0.07	0.57
18	Hybrid	No	15	6.3	0.4	533	2.40	4.25
19	Hybrid	No	14	6.4	0.5	533	5.24	5.48
20	Hybrid	No	22	4.8	0.2	419	3.91	5.86
21	Hybrid	No	10	6.5	0.7	769	1.73	2.90
22	Saucer	Yes	9	6.8	0.8	769	2.84	3.03
23	Hybrid	Yes	4	3	0.8	533	0.16	0.23
24	Saucer	Yes	4	2.5	0.6	297	0.08	0.37

25	Saucer	Yes	2	1.3	0.7	173	0.01	0.06
26	Saucer	No	7	5.8	0.8	998	1.67	1.82
27	Compound	No	19	9.1	0.5	236	7.03	8.40
28	Hybrid	Yes	9	4.2	0.5	297	1.72	1.89
29	Hybrid	Yes	4	2.6	0.7	357	6.24	6.43
30	Hybrid	Yes	14	5.8	0.4	297	0.61	0.73
31	Saucer	Yes	4	2.5	0.6	480	0.04	0.35
32	Hybrid	Yes	5	3.2	0.6	533	0.51	0.68
33	Saucer	No	2	1.8	0.9	297	0.25	0.26
34	Saucer	No	4	2	0.5	297	0.04	0.31
35	Hybrid	Yes	8.2	6.7	0.8	80	1.57	1.76
36	Hybrid	Yes	20	18.6	0.9	84	9.94	10.41
37	Hybrid	No	12.1	3.8	0.3	183	0.49	2.03
38	Hybrid	No	2	1.6	0.8	266	0.17	0.21
39	Saucer	Yes	2.5	2.3	0.9	357	0.14	0.14

Table 1. Measurements of intrusion dimensions. * assumes the intrusion is 5 m thick in areas where it is represented by a single trough-peak doublet. † assumes the intrusion is 44 m thick in areas where it is represented by a single trough-peak doublet.

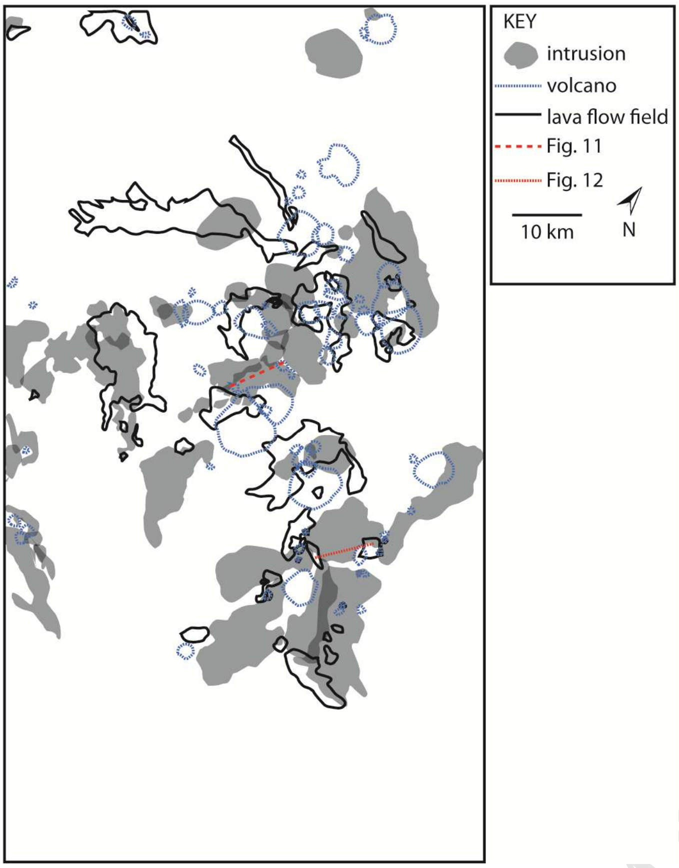
KEY
intrusion
volcano
lava flow field
Fig. 11
Fig. 12
10 km
N

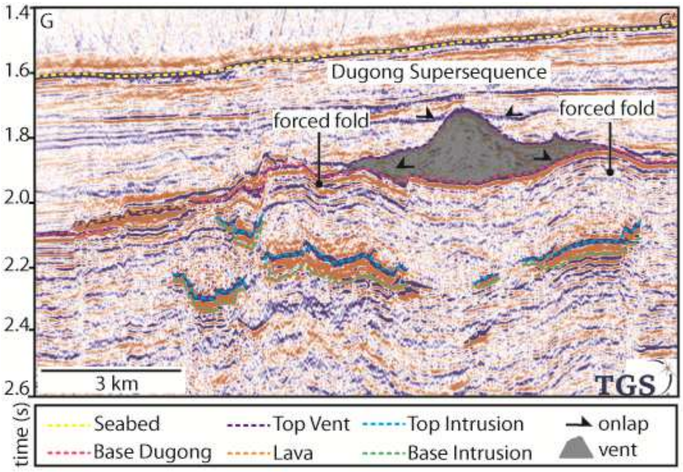

G
G'
Dugong Supersequence
forced fold
forced fold
3 km
TGS
time (s)
1.4
1.6
1.8
2.0
2.2
2.4
2.6
Seabed
Base Dugong
Top Vent
Lava
Top Intrusion
Base Intrusion
onlap
vent

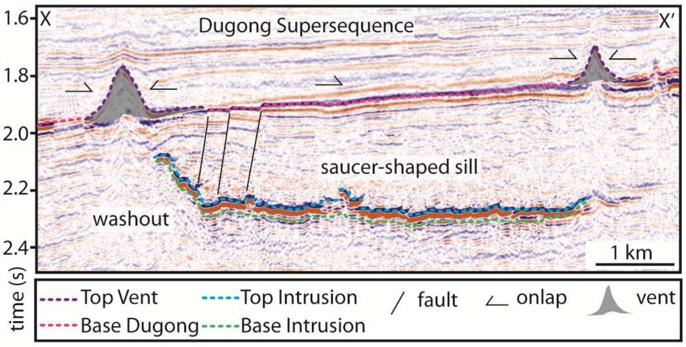
X
X′
Dugong Supersequence
saucer-shaped sill
washout
1 km
1.6
1.8
2.0
2.2
2.4
time (s)
Top Vent
Base Dugong
Top Intrusion
Base Intrusion
fault
onlap
vent

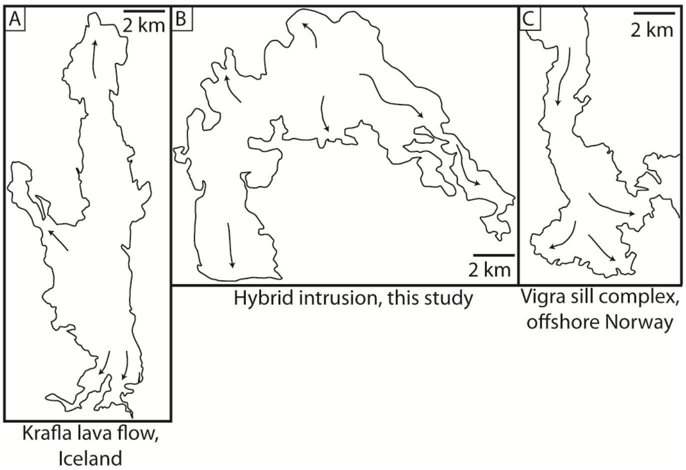
A
2 km
B
2 km
C
2 km
Hybrid intrusion, this study
Vigra sill complex,
offshore Norway
Krafla lava flow,
Iceland

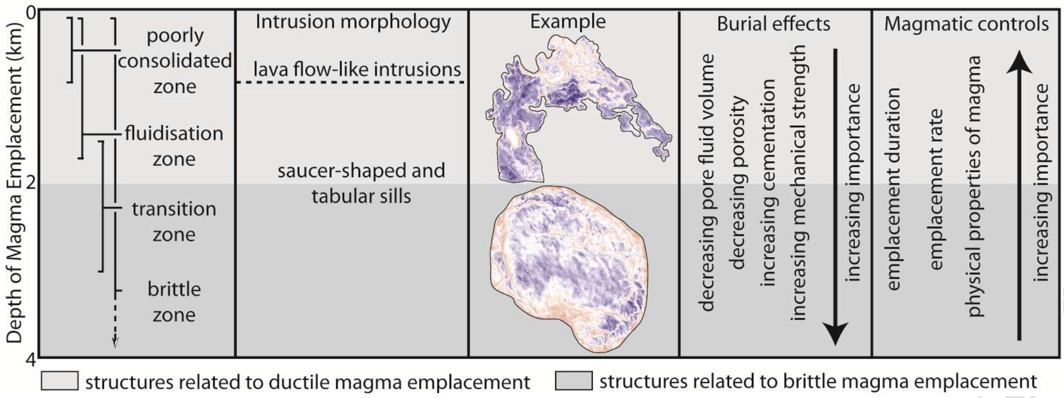
Depth of Magma Emplacement (km)
0
2
4
poorly consolidated zone
fluidisation zone
transition zone
brittle zone
Intrusion morphology
lava flow-like intrusions
saucer-shaped and tabular sills
Example
Burial effects
decreasing pore fluid volume
decreasing porosity
increasing cementation
increasing mechanical strength
increasing importance
Magmatic controls
emplacement duration
emplacement rate
physical properties of magma
increasing importance
structures related to ductile magma emplacement
structures related to brittle magma emplacement

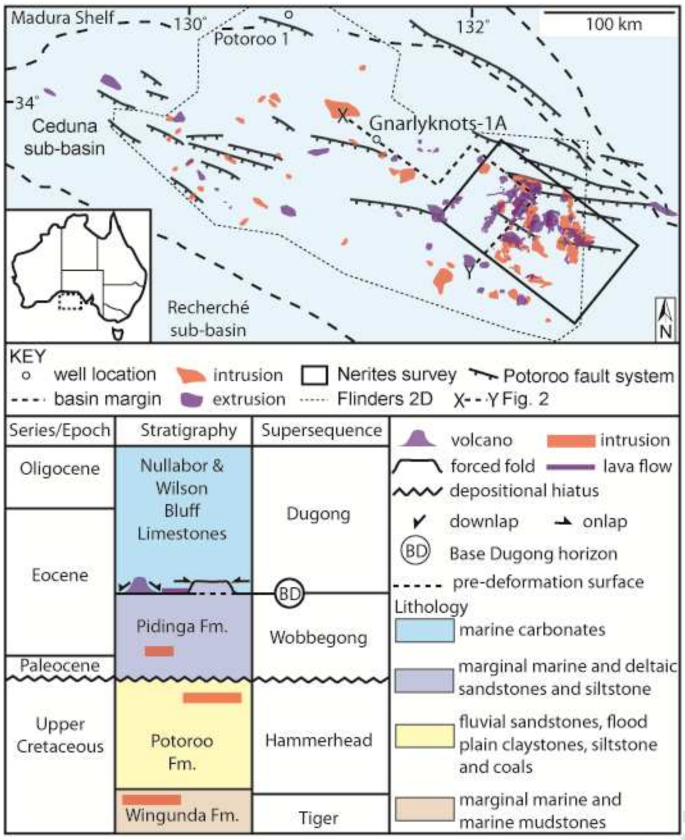
Madura Shelf
130°
Potoroo 1
132°
100 km
34°
Ceduna
sub-basin
Gnarlyknots-1A
Recherché
sub-basin
N
KEY
well location
intrusion
Nerites survey
Potoroo fault system
basin margin
extrusion
Flinders 2D
X- - Y Fig. 2
Series/Epoch
Stratigraphy
Supersequence
Oligocene
Eocene
Paleocene
Upper
Cretaceous
Nullabor &
Wilson
Bluff
Limestones
Pidinga Fm.
Potoroo
Fm.
Wingunda Fm.
Dugong
BD
Wobbegong
Hammerhead
Tiger
volcano
intrusion
forced fold
lava flow
depositional hiatus
downlap
onlap
Base Dugong horizon
pre-deformation surface
Lithology
marine carbonates
marginal marine and deltaic
sandstones and siltstone
fluvial sandstones, flood
plain claystones, siltstone
and coals
marginal marine and
marine mudstones

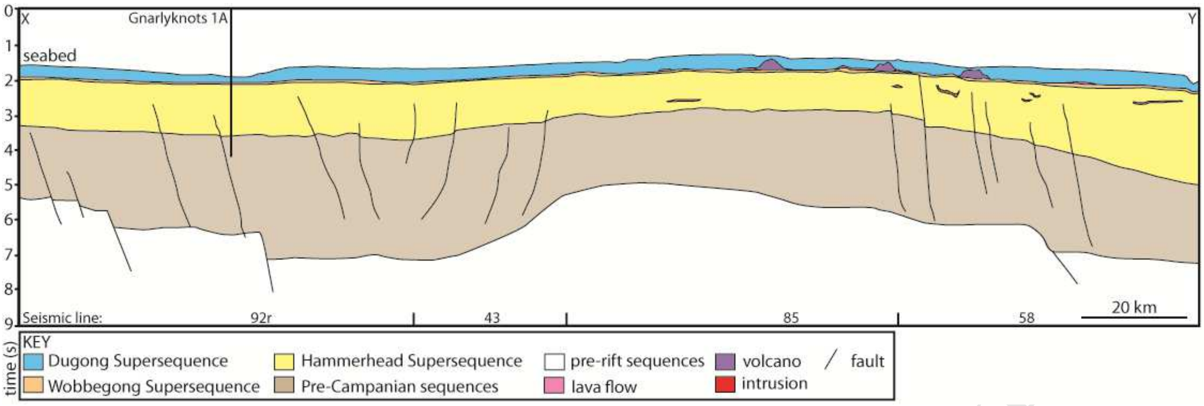
X
Y
Gnarlyknots 1A
seabed
0
1
2
3
4
5
6
7
8
9
time (s)
Seismic line:
92r
43
85
58
20 km
KEY
Dugong Supersequence
Wobbegong Supersequence
Hammerhead Supersequence
Pre-Campanian sequences
pre-rift sequences
lava flow
volcano
intrusion
fault

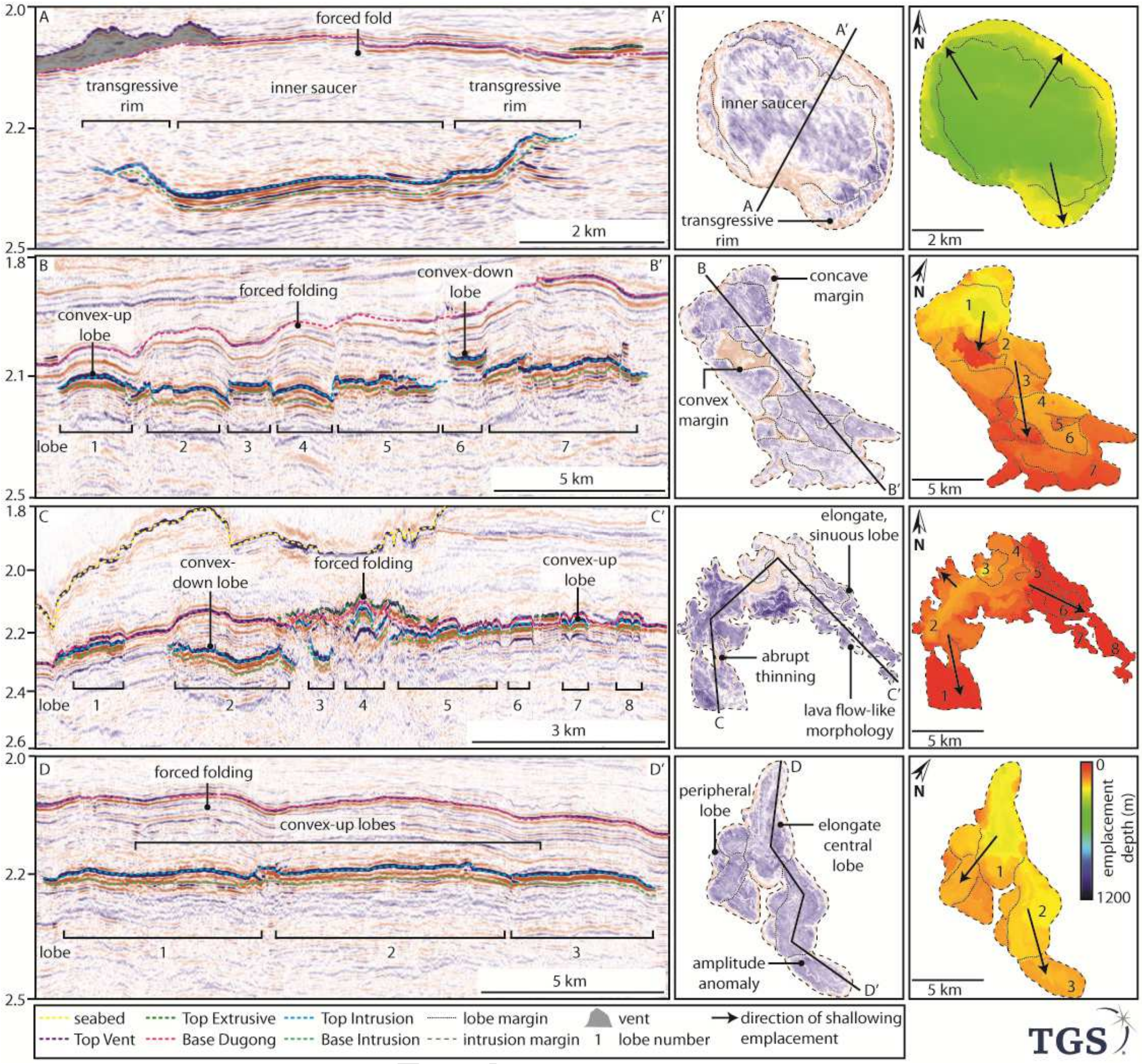

A
A′
forced fold
transgressive rim
inner saucer
transgressive rim
2 km
inner saucer
transgressive rim
N
2 km
B
B′
forced folding
convex-down lobe
convex-up lobe
lobe 1 2 3 4 5 6 7
5 km
concave margin
convex margin
5 km
C
C′
convex-down lobe
forced folding
convex-up lobe
lobe 1 2 3 4 5 6 7 8
3 km
elongate, sinuous lobe
abrupt thinning
lava flow-like morphology
5 km
D
D′
forced folding
convex-up lobes
lobe 1 2 3
5 km
peripheral lobe
elongate central lobe
amplitude anomaly
emplacement depth (m)
0
1200
5 km
seabed
Top Vent
Top Extrusive
Base Dugong
Top Intrusion
Base Intrusion
lobe margin
intrusion margin
vent
1 lobe number
direction of shallowing emplacement
TGS

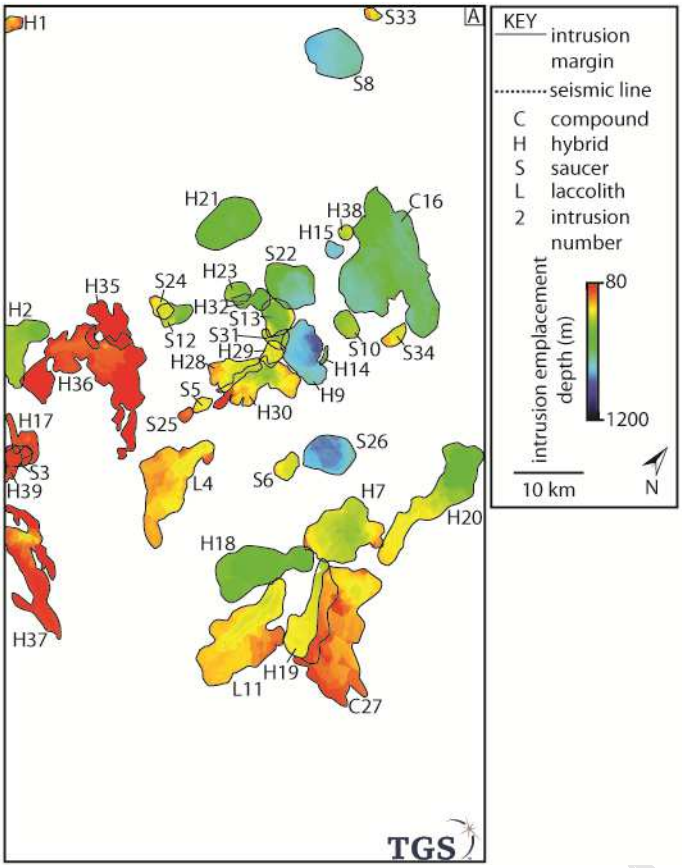
A
H1
S33
S8
H21
H38
C16
H15
S22
H23
H35
S24
H2
H32
S13
S12
S31
H29
S10
S34
H28
H14
H36
H9
S5
H30
S25
H17
S26
S3
H39
L4
S6
H7
H20
H18
H37
H19
L11
C27
TGS
KEY
intrusion margin
seismic line
C compound
H hybrid
S saucer
L laccolith
2 intrusion number
intrusion emplacement depth (m)
80
1200
10 km
N

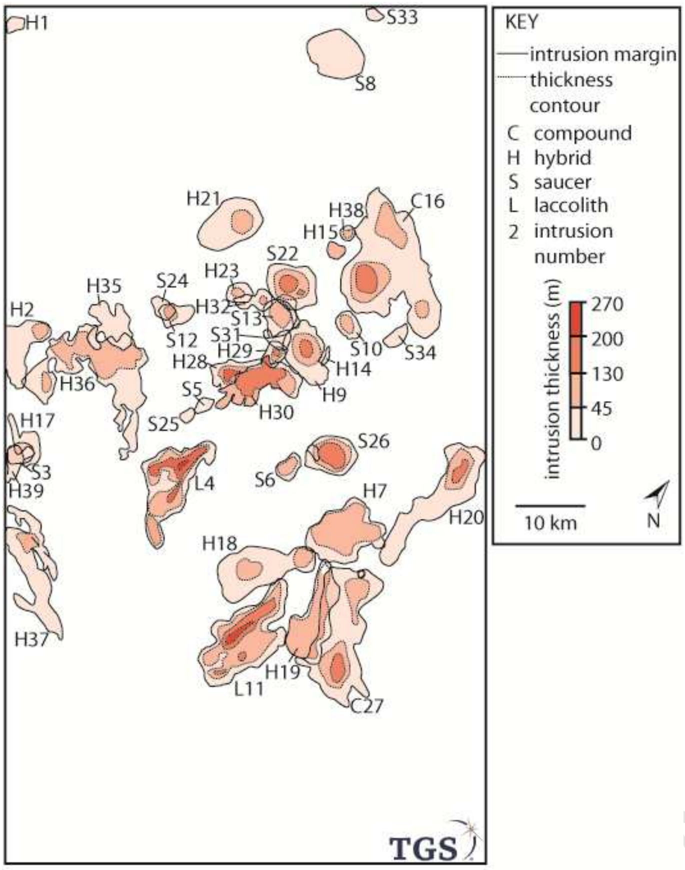

H1
S33
S8
H21
H38
C16
H15
S22
H23
H35
S24
H2
H32
S13
S12
S31
S10
S34
H29
H28
H14
H36
S5
H9
H30
S25
H17
S26
S3
H39
L4
S6
H7
H20
H18
H37
H19
L11
C27
TGS
KEY
intrusion margin
thickness contour
C compound
H hybrid
S saucer
L laccolith
2 intrusion number
intrusion thickness (m)
270
200
130
45
0
10 km
N

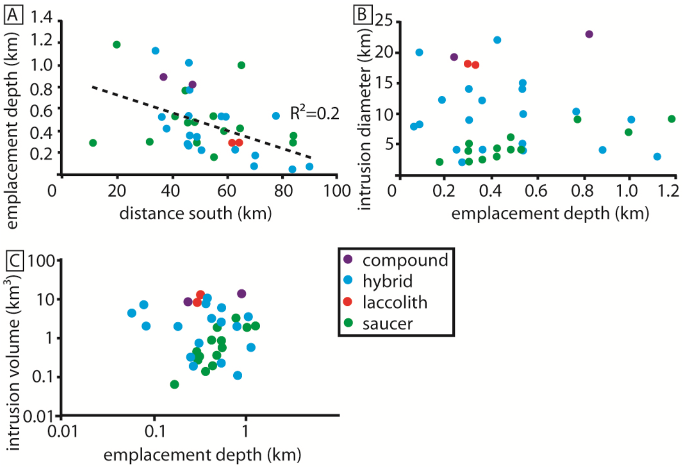
A
emplacement depth (km)
1.4
1.2
1.0
0.8
0.6
0.4
0.2
0
20
40
60
80
100
distance south (km)
R²=0.2
B
intrusion diameter (km)
25
20
15
10
5
0
0.2
0.4
0.6
0.8
1.0
1.2
emplacement depth (km)
C
intrusion volume (km³)
100
10
1
0.1
0.01
0.01
0.1
1
emplacement depth (km)
compound
hybrid
laccolith
saucer

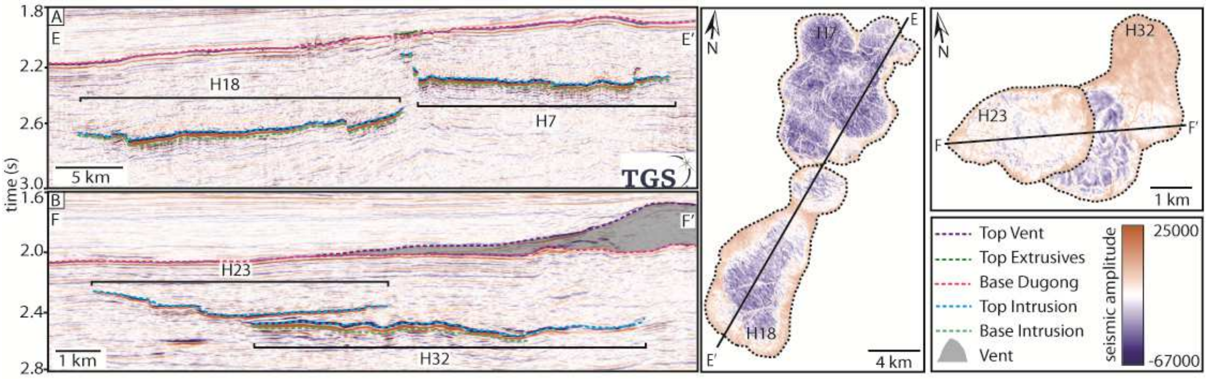

A
E
E'
H18
H7
5 km
TGS
time (s)
B
F
F'
H23
H32
1 km
N
H7
H18
E
E'
4 km
H32
H23
F
F'
1 km
Top Vent
Top Extrusives
Base Dugong
Top Intrusion
Base Intrusion
Vent
seismic amplitude
25000
-67000

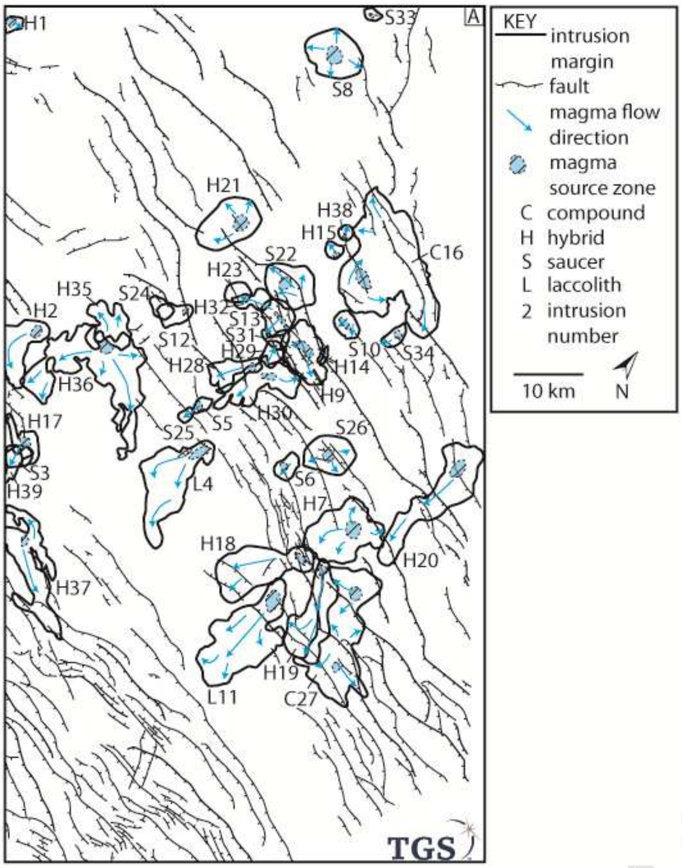
A
KEY
intrusion margin
fault
magma flow direction
magma source zone
C compound
H hybrid
S saucer
L laccolith
2 intrusion number
10 km
N
H1
S33
S8
H21
H38
H15
C16
H23
S22
H35
S24
H2
H32
S13
S31
S12
H29
S10
S34
H28
H14
H36
H9
H30
H17
S25
S5
S26
S3
H39
L4
S6
H7
H18
H20
H37
H19
L11
C27
TGS

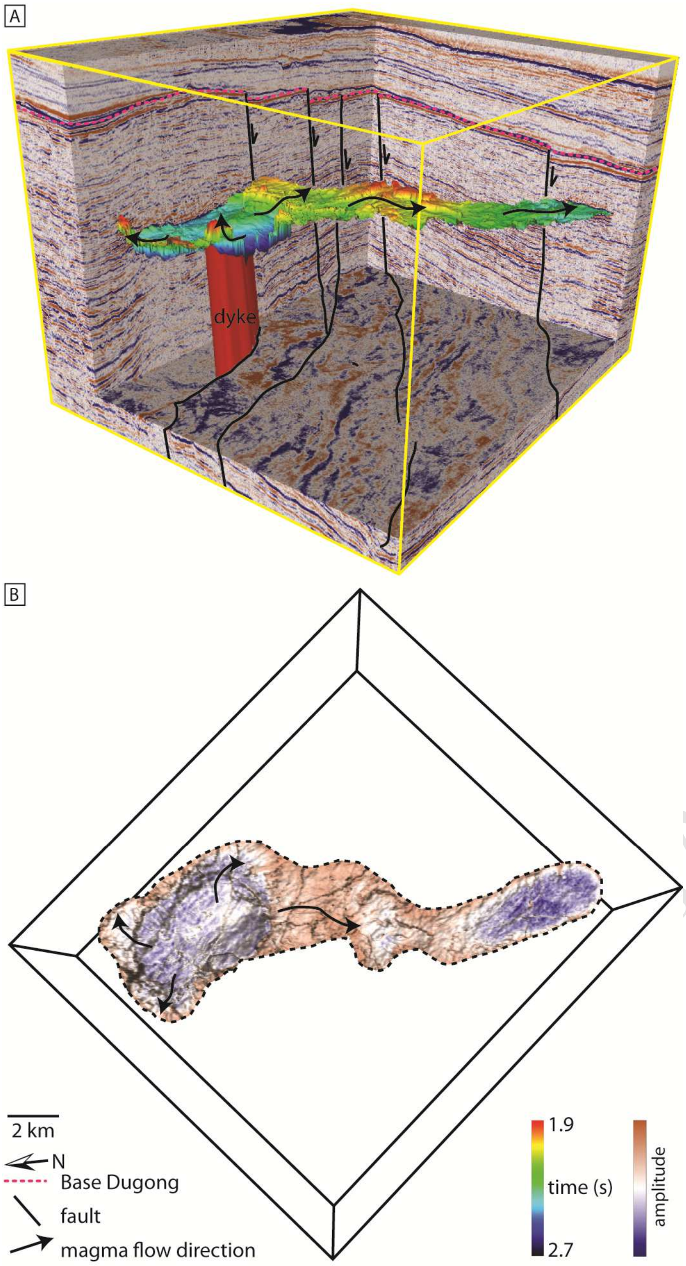
A
dyke
B
2 km
N
Base Dugong
fault
magma flow direction
1.9
time (s)
2.7
amplitude

- We describe magmatic intrusions in a sedimentary basin offshore southern Australia.
- The intrusions are confined to within 1200 m of the paleoseabed.
- The intrusions occur as isolated bodies, suggesting they were fed by dykes.
- High magma ascent rates prevented the dyke-sill transition deep in the basin.